sensors

MDPI

Paper

c-axis textured, 2-3µm thick $Al_{0.75}Sc_{0.25}N$ films grown on chemically formed TiN/Ti seeding layers for MEMS applications

Asaf Cohen[1], Hagai Cohen[2], Sidney R. Cohen[2], Sergey Khodorov[1], Yishay Feldman[2], Anna Kossoy[2], Ifat Kaplan-Ashiri[2], Anatoly Frenkel[3], Ellen Wachtel[1], Igor Lubomirsky[1] * and David Ehre[1] *

[1]Department of Molecular Chemistry and Materials Science, Weizmann Institute of Science, Rehovot, 7610001, Israel
2Department of Chemical Research Support, Weizmann Institute of Science, Rehovot, 7610001, Israel;
[3]Department of Materials Science and Chemical Engineering, Stony Brook University, NY

* Correspondence: DE- david.ehre@weizmann.ac.il; IL- igor.lubomirsky@weizmann.ac.il

Abstract:

A protocol for successfully depositing [*00l*] textured, 2-3µm thick films of $Al_{0.75}Sc_{0.25}N$, is proposed. The procedure relies on the fact that sputtered Ti is (00*l*)-textured ***α***-phase (hcp). Diffusion of nitrogen ions into the α-Ti film during reactive sputtering of $Al_{0.75}Sc_{0.25}N$ likely forms a (111)-oriented TiN intermediate layer . The lattice mismatch of this very thin film with $Al_{0.75}Sc_{0.25}N$ is ~ 3.7% , providing excellent conditions for epitaxial growth. In contrast to earlier reports, the $Al_{0.75}Sc_{0.25}N$ films prepared in the current study are Al-terminated. Low growth stress (< 100 MPa) allows films up to 3 µm thick to be deposited without loss of orientation or decrease in piezoelectric coefficient. An advantage of the proposed technique is that it is compatible with a variety of substrates commonly used for actuators or MEMS, as demonstrated here for both Si wafers and D263 borosilicate glass. Additionally, thicker films can potentially achieve increased piezoelectric stress/strain by permitting application of higher voltage, but without increase in the magnitude of the electric field.

Citation: Lastname, F.; Lastname, F.; Lastname, F. Title. *Sensors* **2022**, *22*, x. https://doi.org/10.3390/xxxxx

Academic Editor: Firstname Lastname

Received: date
Accepted: date
Published: date

Publisher's Note: MDPI stays neutral with regard to jurisdictional claims in published maps and institutional affiliations.

Keywords: Aluminum scandium nitride, sputtering, seeding layer, texture, piezoelectric

1 Introduction

In the search for lead-free, Si-microfabrication-compatible piezoelectric materials, thin films of scandium-doped aluminum nitride (Al,Sc)N are of great interest for use in actuators[1], energy harvesting[2] and micro-electromechanical-systems (MEMS). While the piezoelectric response of AlN increases upon doping with Sc[3, 4], difficulties are encountered during film preparation because, as bulk solids with completely different structures and large differences in cation radii, ScN (rock salt , cubic) and AlN (wurtzite , hexagonal) are immiscible[5]. Consequently, (Al,Sc)N is inherently thermodynamically unstable and prone to phase segregation[3]. Film preparation is further complicated by the technological requirement for polar (001) or (00$\bar{1}$) out-of-plane texture, which is achieved using a seeding layer.

To promote growth of textured (Al,Sc)N films (*i.e.*, $Al_{1-x}Sc_xN$, x<0.4), the seeding layer should satisfy at least two requirements: **a)** close epitaxial match to the growing film[6, 7] ; and **b)** low surface roughness to prevent secondary nucleation [6]. The most common preparation protocol uses reactive DC sputtering onto textured seeding layers of (111) fcc or (110) bcc metals[6-8], *e.g.*, Au, Pt, or Mo. These metals are chemically inert towards both $\boldsymbol{N_2}$ and (Al,Sc)N, and display lattice mismatch to the (001) planes of (Al,Sc)N of 7.5%, 10.8% and 12.4% respectively[6]. It was observed that even when growing films of (Al,Sc)N initially display strong [00*l*] texture, orientation is often lost once film thickness exceeds a few hundred nm[3]. The loss of orientation is attributed to local stress/strain[3] induced by the lattice mismatch[6] during deposition and/or large substrate surface roughness[6],[9]. These characteristics, combined with the thermodynamic instability of (Al,Sc)N, are thought to promote Sc segregation to the grain boundaries, further accelerating phase separation and/or loss of orientation[3, 10]. (001)-oriented hcp α-Ti or (111) rock-salt TiN may constitute a better seeding layer than fcc or bcc metals, since these Ti-based materials can provide smaller epitaxial mismatch to (Al,Sc)N. However, earlier studies of $< \boldsymbol{1\mu m}$ thick sputtered undoped AlN films, reported that fcc metal seeding layers resulted in well textured films, while bcc or hcp lattices did not [6]. On the other hand, refs. [7],[11], [12] found that α-Ti and TiN are indeed suitable seeding layers for AlN or (Al,Sc)N films . Given the large variety of parameters controlling the outcome of reactive sputtering deposition of Sc-doped AlN, e.g., Sc concentration, number of sputtering targets, time, temperature, substrate, seeding layer(s), Ar/N_2 plasma gas pressure and volume ratio, one can begin to account for the broad range of (well-oriented) film thicknesses and strength of electromechanical coupling that have been reported[12-16].

The present work proposes replacing a chemically inert seeding layer with TiN/α-Ti. Our procedure takes advantage of the observation that DC sputtering of Ti metal produces well (00*l*)-oriented films on a variety of substrates. **[17-19]** However, while (00*l*)-textured $\boldsymbol{\alpha}$-Ti presents ~5.1% lattice mismatch to (Al,Sc)N, this is reduced to ~3.7% for the case of (111) oriented TiN. (See Supplementary, Section 1). In the following, we provide evidence for the *in situ* formation of a few nm thick, TiN films during reactive sputtering of $Al_{1-x}Sc_xN$, (x=0.25) with nitrogen plasma at the surface of a deposited (00*l*)-textured $\boldsymbol{\alpha}$-Ti layer. The proposed method leads to stable, piezoelectric (00*l*)-textured films with thickness up to 3 μm.

2 Materials and Methods

6N purity gases (N_2, argon, O_2) were used, supplied by Gas Technologies, Israel. Hydrofluoric acid (HF), organic solvents, acetone and isopropyl alcohol (IPA) were semiconductor grade (CMOS, Sigma Aldrich).

2.1 Deposition of titanium films

50 nm thick titanium films were deposited by DC sputtering for 10 min while maintaining the substrate at room temperature. Two-inch diameter substrates were used: (100) \p- Si silicon wafers (10-30 ohm·cm, University Wafers, thickness 250±25μm) and D263 borosilicate glass (SCHOTT, thickness 500±50μm). Substrates were cleaned with solvents in order of increasing polarity: acetone, isopropyl alcohol, deionized water. Dilute (4vol%) HF was then used to remove the native oxide layer as well as surface contaminants. The substrates underwent argon and oxygen plasma cleaning to remove organic contaminants in the sputtering chamber at 10mTorr pressure with oxygen/argon ratio 1:1 by volume. The Ti films were deposited from a 2-inch diameter, 5N purity Ti target, (Abletarget, China) by DC magnetron sputtering (ATC Orion Series Sputtering Systems, AJA International, Inc.) with power level 150W. The distance between the magnetron and the substrate was 24 cm; the pressure of Ar in the chamber during deposition was 5 mTorr. For study of

the diffusion of nitrogen into the surface of the α-Ti films, they were exposed to nitrogen plasma at 5mTorr pressure for 30 min at 673K, using the AJA glow discharge option.

2.2 **Deposition of $Al_{0.75}Sc_{0.25}N$ thin films**

$Al_{0.75}Sc_{0.25}N$ films were deposited by DC reactive sputtering from $Al_{0.75}Sc_{0.25}$ metal alloy targets onto the Ti-seeding layers prepared as described above. 250 W power was applied to a 3-inch diameter magnetron loaded with 5N purity metal alloy targets (Abletarget, China). The pressure in the chamber was 5mTorr and the ratio between argon and nitrogen was 1:4 by volume. The samples listed in Table 1 were prepared with deposition temperature profile: 30min at 673K followed by sputtering for 8-13hrs at 523K.

Table 1. Identification of the $(Al, Sc)N$ film samples deposited as described in section 0. The Stoney formula was used for calculation of residual in-plane film stress, $\sigma = \frac{E_s h_s^2}{6(1-\nu_s)h_f}\left(\frac{1}{R} - \frac{1}{R_0}\right)$, where E is the Young's modulus; h is thickness; ν is the Poisson ratio; R is cantilever radius of curvature following deposition; R_0 is the initial radius of curvature. Subscripts s, f refer to the substrate and thin film respectively.

Title	Substrate	Under-layer	AlScN h_f [µm]	Film Stress σ [MPa]
ASN1	Silicon (100)	50nm Ti	3±0.1	62.5 ± 9.6
ASN2	Borosilicate glass (D263)	50nm Ti	3±0.1	80.7±12.5
ASN3	Silicon (100)	100nm Al+50nm Ti	2±0.1	56.3 ± 8.7

2.3. **Measurement of the piezoelectric coefficient and pyroelectric response**

The resulting films were covered with a 50nm thick titanium layer, which served as the top electrode. Wafers with [substrate\Ti\$Al_{0.75}Sc_{0.25}N$\Ti] film stacks were cut into rectangular (1 cm wide and 2-4 cm long) plates. These were mounted as cantilevers in a deflection monitoring setup (***viz.,*** ref. [20]) and bias was applied between the top and bottom Ti layers. The piezoelectric coefficient was calculated from the stress induced in the cantilever due to voltage application. The stress was calculated using the Stoney formula under the assumption of purely cylindrical bending (zero Gaussian curvature). The pyroelectric response was measured with the (Chynoweth) periodic temperature change method using a modulated IR laser (wavelength 1560 nm, 12 W/cm^2 OSTECH, Germany) operating at 17 kHz [21-23]. In order to ensure maximum radiation absorption, the 2 mm diameter Ti contacts prepared for these measurements were covered with carbon black.

2.4 Film Characterization –SEM, AFM, EDS, XRD, XPS

Film thickness was measured on sample cross sections with a scanning electron microscope SEM (Zeiss Sigma 500, and Zeiss Supra 55VP SEMS, 4-8keV). SEM images were also used to estimate mean grain size and morphology of both the surface and cross-section. Nanoscale topography maps were acquired with an atomic force microscope (Multimode AFM (Bruker) in the **p**eak-**f**orce **t**apping mode, using a PNP-TRS probe). Elemental analysis was performed by energy dispersive X-ray spectroscopy (EDS) using a four quadrant detector (Bruker, FlatQUAD) installed on the Zeiss Ultra 55 SEM. Accelerating voltage was 8kV. X-ray diffraction (XRD) patterns were collected with a TTRAX III diffractometer

(Rigaku, Japan) in Bragg-Brentano mode. To characterize film texture, pole figures were recorded at the relevant Bragg angle using an Euler cradle plus a Shultz slit for limiting the footprint of the extended X-ray illumination spot arising from sample tilt. The intensity and line width of the $Al_{0.75}Sc_{0.25}N$ (002) diffraction peak monitored the quality of ***c***-axis texture. The diffracted intensity of (100) and (011) pole figures was too weak to be detected, permitting an estimate that they are at least 500 times weaker than the (002) peak. Film in-plane stress was deduced from the change in the wafer curvature, before and after film deposition, using a DektakXT stylus profilometer. Since the $Al_{0.75}Sc_{0.25}N$ film was by far the thickest in the stack, in-plane stress was calculated neglecting the mechanical properties of other layers. X-ray photoelectron spectroscopy (XPS, Kratos AXIS-Ultra DLD spectrometer with monochromatic Al K_α source at low power, 15-75W) was used for surface chemical analysis as a determinant of TiN layer formation. Independently, XPS was used as a non-contact probe of the $Al_{0.75}Sc_{0.25}N$ layer pyroelectric response[24], for which the sample temperature, (RT or when cooled by liquid nitrogen , (233-283K)), was monitored by a thermocouple located in close proximity to the back side of the sample. Repeated scans were made at each temperature in order to accurately quantitate binding energies upon temperature stabilization at the surface. The sign of the pyroelectric coefficient and the temperature dependence of a relevant XPS peak (in our case N 1s) are both reliable monitors of material polarity. **[21, 24-26].** These measurements are not sensitive to details of the material surface, and consequently they are the methods of choice in this report.

3 Results

3.1 Formation of TiN on a Ti seeding layer

Sputtered Ti is known to grow as α-phase (hcp) with preferred (001) orientation [17-19]. 50 nm thick Ti films were deposited as a seeding layer by DC magnetron sputtering on both types of substrates as described above (section 2.1). According to the XRD patterns (Figure 1), the films are indeed α −Ti with (00*l*) texture: the (002)-diffraction peak dominates the diffraction patterns with peak width $\Delta 2\Theta$ ~0.55° for both substrates.

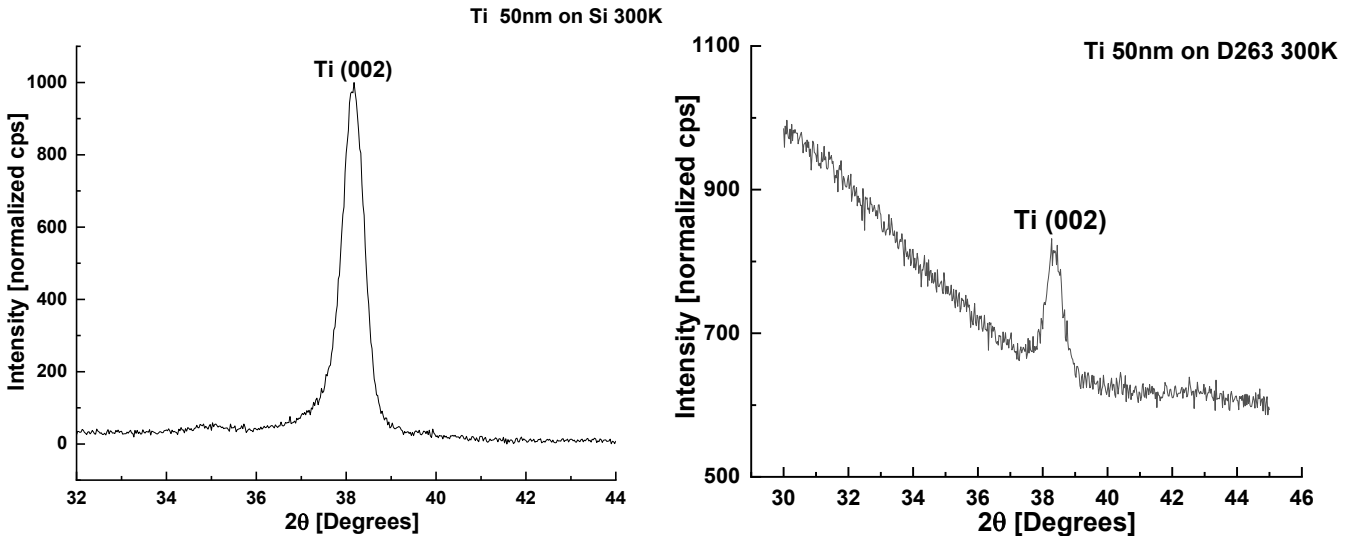

(a) (b)

Figure 1. XRD patterns of 50nm thick layers of Ti deposited at 300K on (a) (100) Si wafers and (b) D263 borosilicate glass, demonstrating strong 00*l* texture.

To investigate the putative formation of (111) oriented TiN on the α-Ti seeding layer (epitaxial relationships are presented in Supplementary Figure S1), sputtered Ti films were exposed to a glow discharge nitrogen plasma at 673K for 30 min. Under these conditions of time and temperature, XRD could not detect the presence of TiN. (see Supplementary Section S2 for more successful alternative sputtering time and temperature). However, the film surface was then investigated with XPS: peaks at 396 eV and 400 eV (both N 1s) and 457 eV (Ti 2p), which can be assigned to oxidized TiN[27, 28], were observed. Oxidation presumably occurred during transfer of the films from the sputtering system to the XPS chamber. Following removal of ~1nm from the surface layer *via* argon sputtering within the XPS chamber, these peaks were 'replaced' by those associated with TiN, 397eV (N 1s) and 455 eV (Ti 2p) [27-29]. With extended argon sputtering time, a gradual transition from TiN to metallic Ti was observed, until the Si substrate was eventually exposed. From the calculated profile of nitrogen atomic concentration *vs* time (Figure 2c), we estimate the TiN layer, formed upon exposure of Ti to nitrogen plasma, to be significantly less than 10 nm thick. This thin layer is likely created *via* nitrogen diffusing into the Ti metal, similar to industrial plasma nitriding [30, 31]

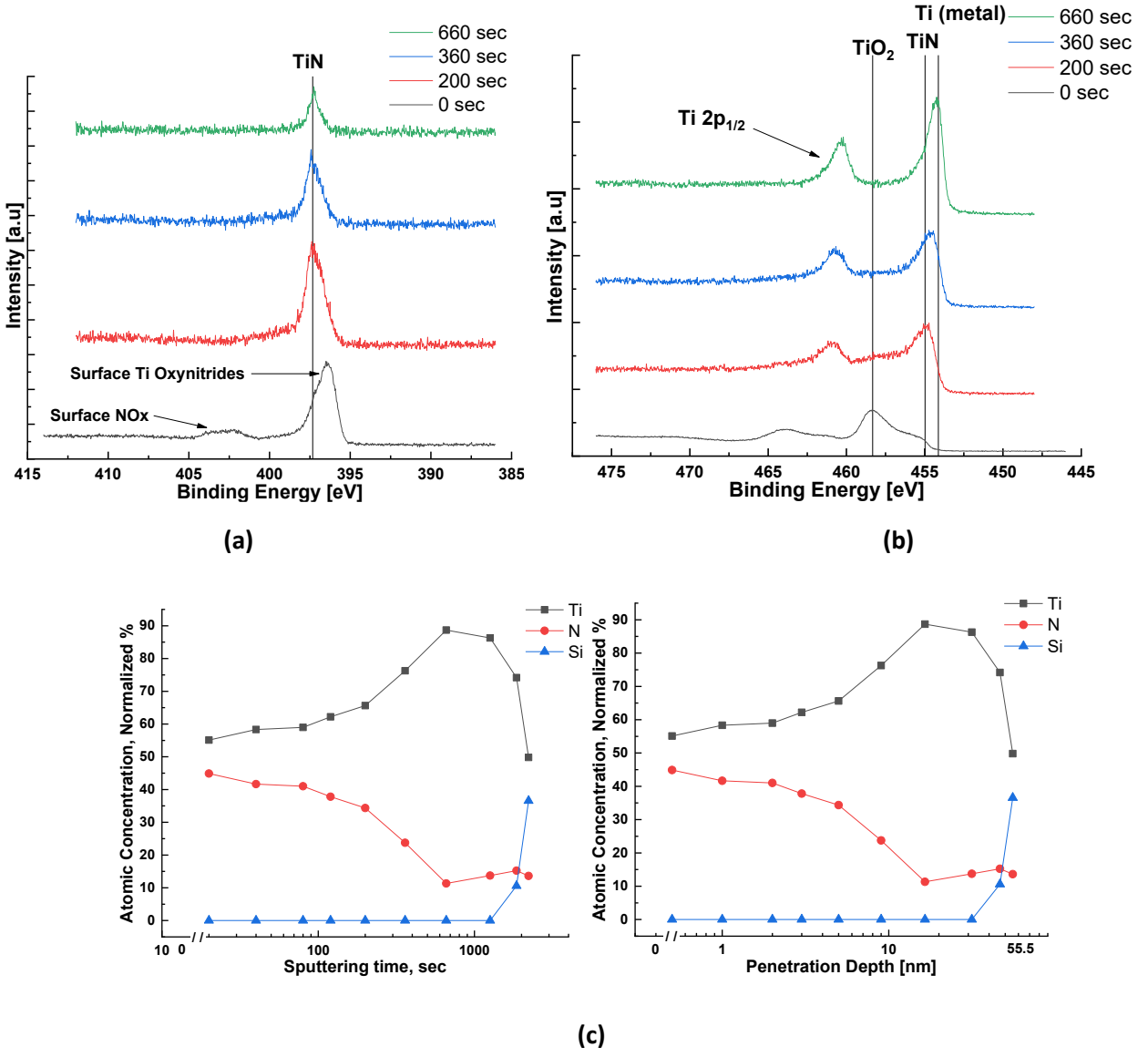

Figure 2. XPS windows of nitrogen N 1s (a) and titanium Ti 2p (b) from the surface of a 50 nm titanium layer deposited on a (100) silicon substrate, and subsequently exposed to nitrogen plasma at 673K; (c) Normalized atomic concentrations of N, Ti, and Si as a function of argon sputtering time in the XPS chamber; the sputtering

rate is estimated to be ~$2.5 \times 10^{-2}\ \frac{nm}{sec}$. Using this sputtering rate, an equivalent graph of atomic concentrations of Ti and N as a function of depth from the layer surface is also included in (c).

AFM images revealed significant smoothing of the Ti layer surface upon formation of TiN (Figure 3). The root mean square roughness of the as-deposited Ti films over an area of 750 x 750 nm² was 1.1 nm; reaction with nitrogen plasma reduced the roughness to 0.68nm, which is favorable for the growth of textured (Al,Sc)N[6].

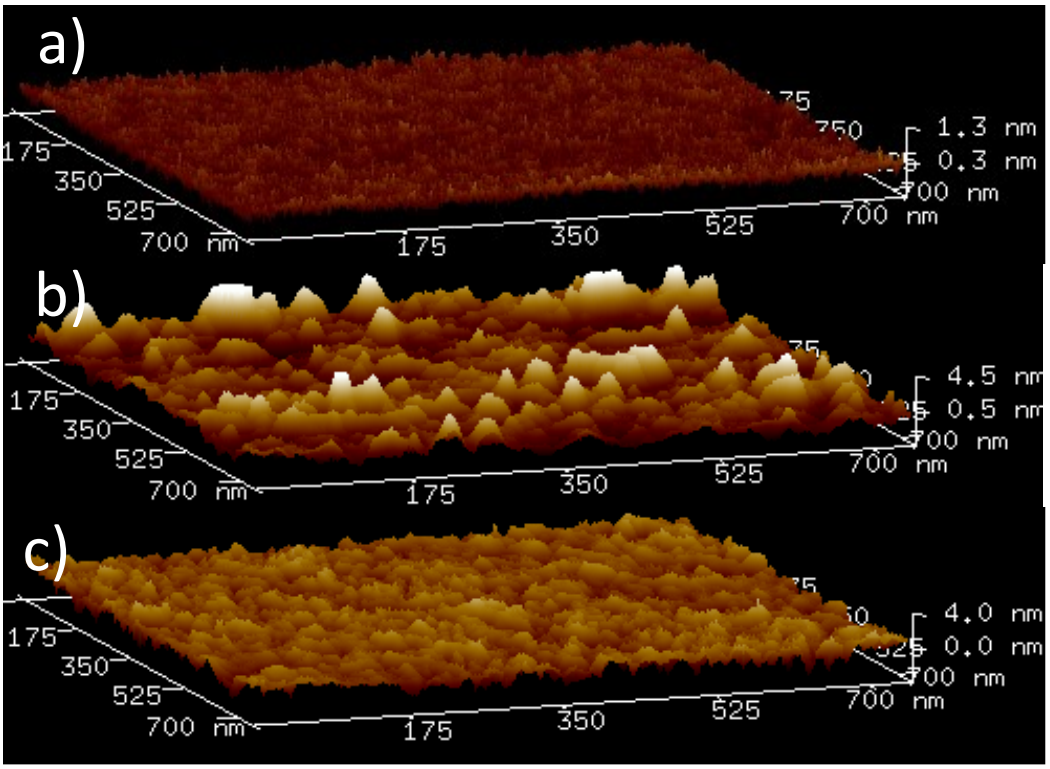

Figure 3. AFM images of: a) a (100) silicon wafer following cleaning procedures as described in the Materials and Methods section; b) 50 nm thick Ti film deposited on the wafer at 300K; c) the same film following exposure to N_2 plasma at 673K for 30 min.

3.2 Reactive sputtering of AlScN

Thin films of $Al_{0.75}Sc_{0.25}N$ were deposited as described in section 0 on both (100) Si wafers and D263 glass substrates coated with 50±10 nm (001)-textured Ti. Without breaking the vacuum after the deposition of Ti seeding layers, the substrates were then heated in the sputtering chamber to 673±10 K. Reactive DC sputtering from a metallic alloy target, $Al_{0.75}Sc_{0.25}$, was performed for 30 min in the nitrogen/argon plasma (see section 0). Deposition at 3.5 to 4 nm/min was then continued at 523K for 8-13 hrs depending on the desired film thickness (2-3 μm), (Supplementary Section S3; Figures S3, S4). Irrespective of the substrate, (100)-Si or D263 borosilicate glass, films up to 3 μm thick were produced (**Error! Reference source not found.**, Figure 4 and Figure 5). Although metal stoichiometry of the deposited films may differ from that of the alloy target, EDS showed negligible change, *i.e.*, $Al_{0.7438}$, $Sc_{0.2562}$ (Also see Supplementary, Section S3). The XRD patterns of the $Al_{0.75}Sc_{0.25}N$ films were dominated by a strong (Al,Sc)N wurtzite (002) diffraction peak at $2\theta \approx 35.5°$, peak width $\Delta 2\theta \approx 0.31 \pm 0.01°$. Pole figures collected for this peak from films grown on both substrates (Figure 4a,b and Figure 5a,b) attest to c-axis texture. We note that the pole figure measured for the asymmetric (103) diffraction peak further supports this claim (Supplementary, Section S3; Figure S5). By fitting a Gaussian profile to a

superposition of (002) pole figure cross sections with different values of the in-plane rotational angle, beta, an equivalent rocking curve FWHM=5.0 ± 1.0° for 3μm (Al,Sc)N films on Si is obtained. (100),(101) diffraction peaks were of negligible intensity [32]. Diffraction characteristic of phase-separated ScN (rock-salt) was not detected [33].

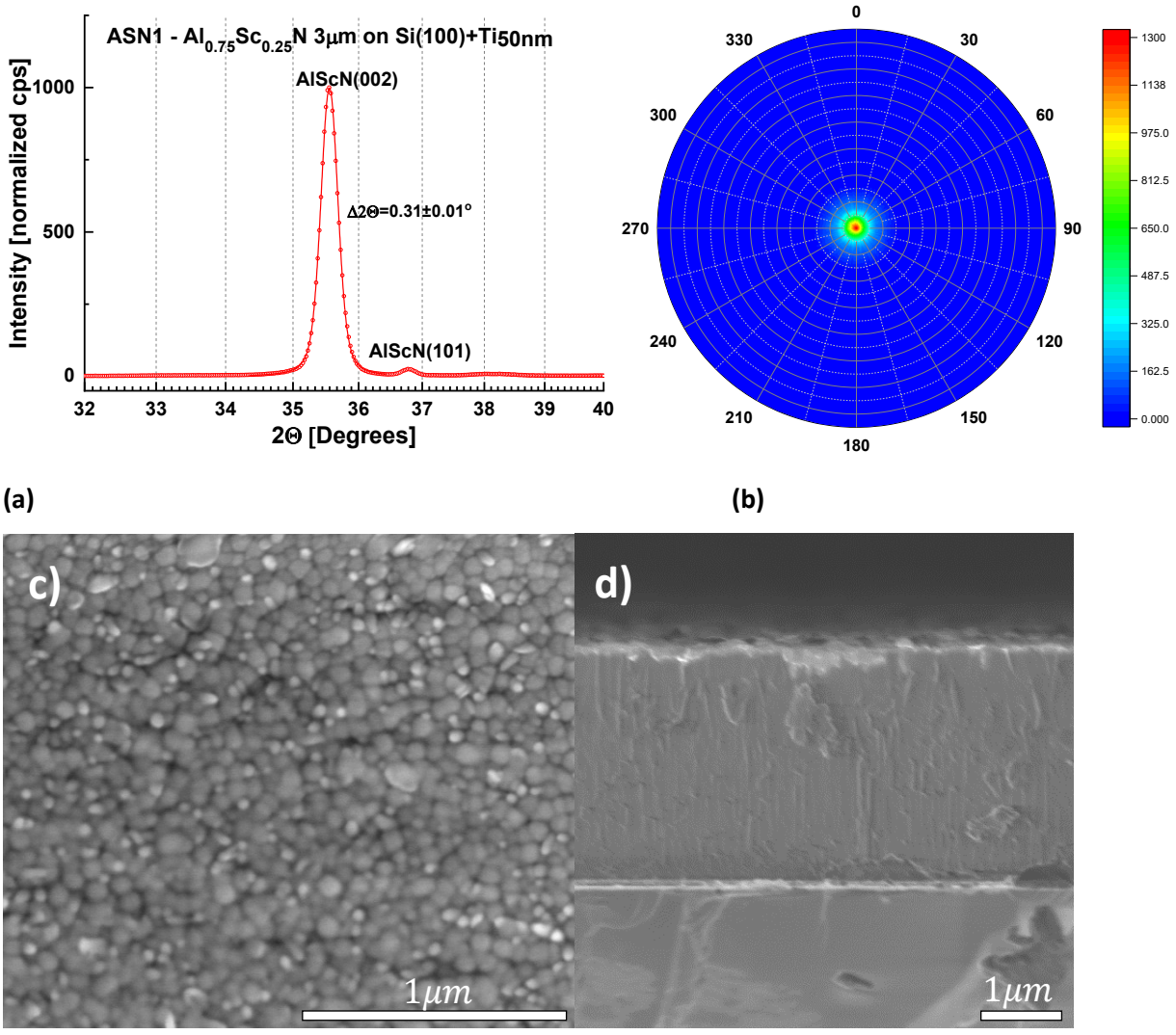

Figure 4. Structural characterization of sample ASN1 (see Table 1) (a,b) XRD pattern and pole figure of the (002) Bragg-peak at 2θ=35.55° ,$\Delta 2\theta$ =0.31±0.01°; (c, d) SEM images of the surface and cross-section of sample ASN1 showing pebble-like grains at the surface (mean transverse dimension, 84nm, as determined by the lineal intercept method) and columnar growth, respectively.

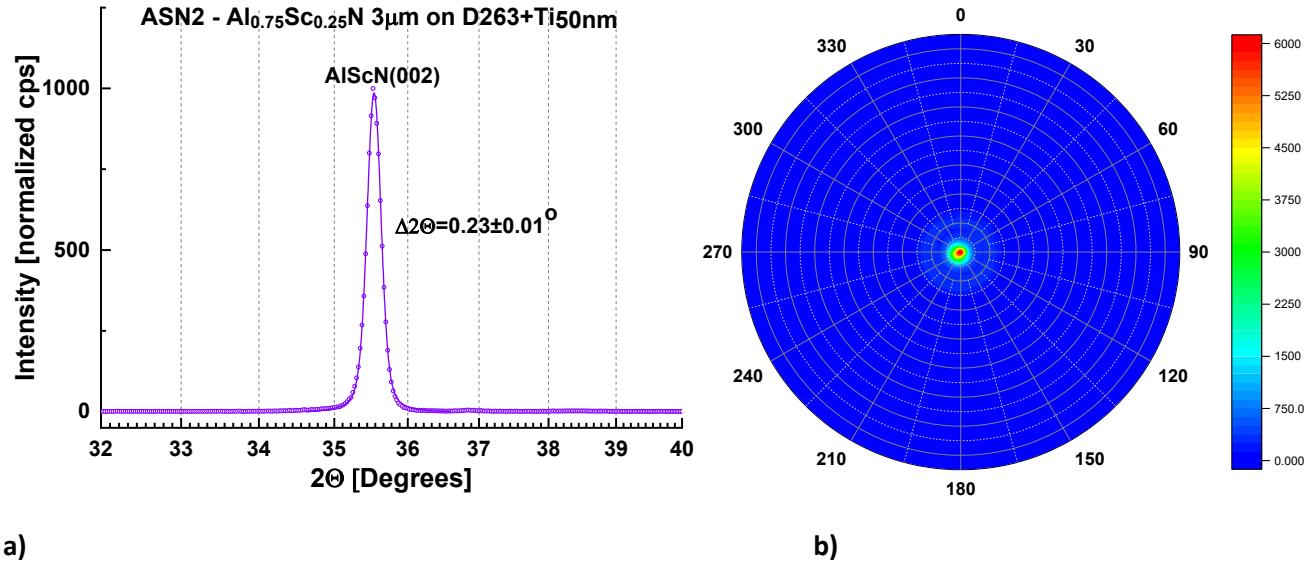

Figure 5. Structural characterization of sample ASN2 (see **Error! Reference source not found.**). (a,b) XRD pattern and pole figure of the (002) Bragg-peak: 2θ=35.54 °,$\Delta 2\theta$ =0.23±0.01°; (c, d) SEM images of the surface and cross section showing pebble-like grains at the surface , mean transverse size 101nm (as determined by the lineal intercept method) and uniform columnar growth, respectively. Misoriented grains are more prevalent in the SEM image of ASN2 as compared to ASN1.

Scanning electron microscope (SEM) images of the film surfaces show pebble-like grains with mean transverse dimension ~85-100 nm (Figure 4c, Figure 5c). For five Si wafers, surface contamination and misoriented, pyramidal grains occupy < 6% of the area as determined from replicate measurements. It was found that film quality was not modified by the presence of a 100 nm thick Al layer introduced to promote relaxation of the compressive stress typical of sputtered (Al,Sc)N [34-36] (Figure 6). Compressive stress in all films, with or without an Al stress relaxation layer, was < 100 MPa, as calculated from the change in wafer curvature , using the Stoney formula [Table 1] and indicating that the Ti\TiN seeding layer supports low deposition stress. EDS elemental mapping demonstrates homogenous distribution of Al and Sc, with no indication of ScN segregation (Figure 7).

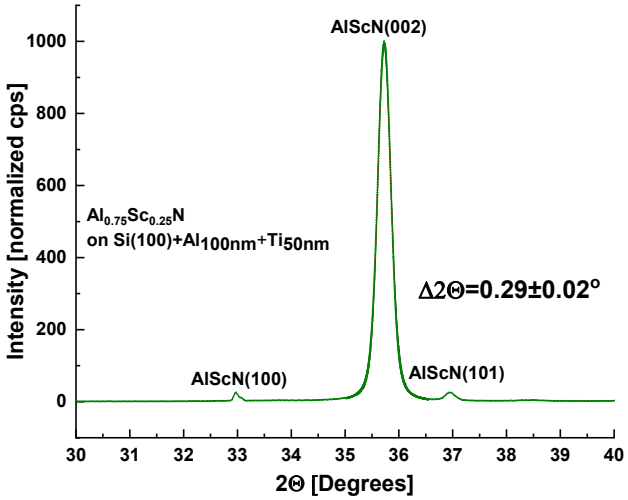

Figure 6. XRD pattern of sample ASN3 grown on (100) Si with a Ti seeding layer and with a stress-relieving Al layer (see Table 1).

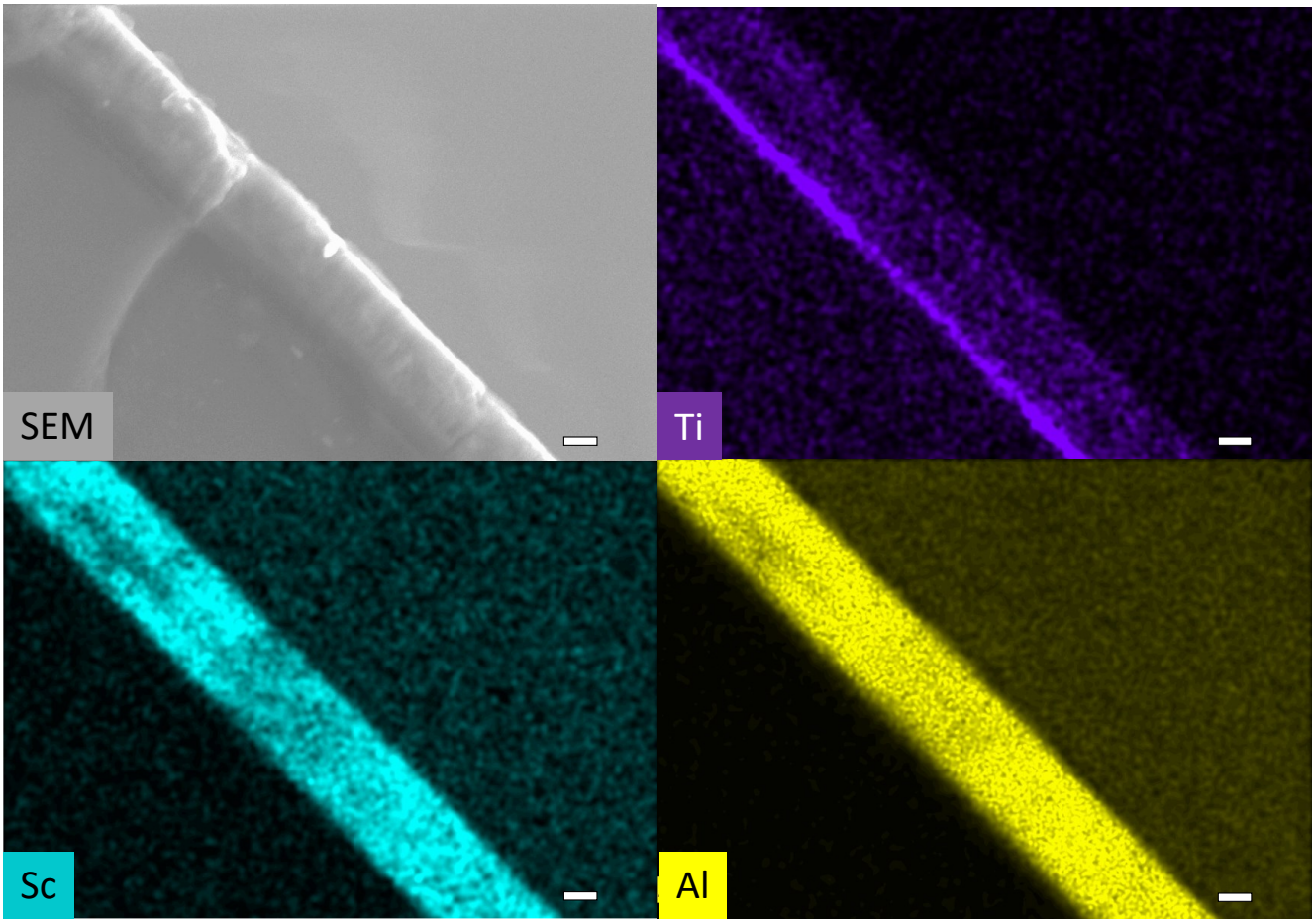

Figure 7. SEM image and elemental mapping of a cross section of a $Al_{0.75}Sc_{0.25}N$ thin film deposited on a Si wafer covered with a Ti /TiN seeding layer. All scale bars designate 1µm. Electron beam energy during the acquisition was 8 keV.

3.3 Pyroelectric measurements

To determine whether the polar axis is directed toward, or away from, the substrate in sample ASN1, *i.e.* to distinguish between [001] and [00$\bar{1}$] orientations, we measured the pyroelectric effect with PTC-[21, 25] and with XPS[24, 37, 38]-based methods (section 0). The PTC measurements revealed that the film pyroelectric coefficient is $\alpha_f = -13.9 \pm 0.1\ [\mu C/m^2K]$ (Figure 8; and Supplementary Section 5)[25], which is close to that previously reported for this composition (25% Sc) [39]. However, in our case α_f is negative. In the XPS measurements, the N 1s peak shifts upon heating to lower energies (and *vice versa*) (**Figure 9**) providing additional support for the negative pyroelectric response. The sign of the pyroelectric response suggests that the films are [001] oriented, *i.e.* the top surface is Al-terminated. This is in contrast to previous reports of films grown on inert metallic seeding layers, all of which are N-terminated [40];[41];[42]. On the other hand, detecting Al-terminated films is consistent with the proposed nucleation mechanism *i.e.*, the epitaxial growth of (Al,Sc)N wurtzite structure begins from an N-terminated face of TiN.

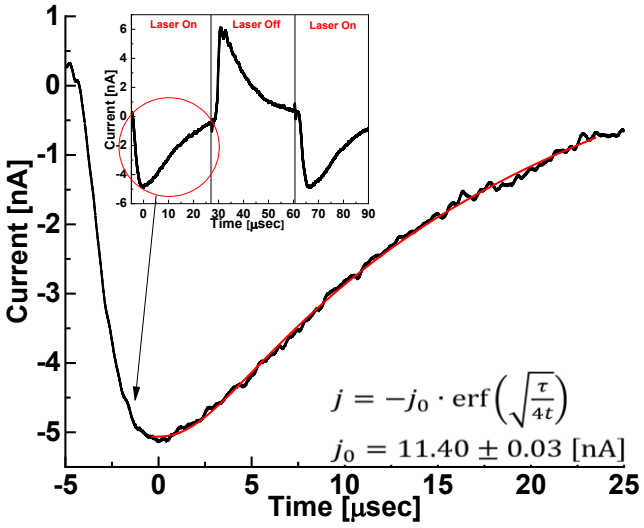

(a)

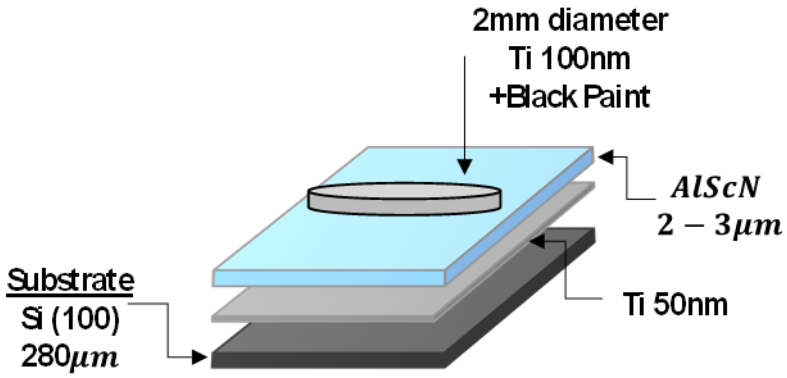

(b)

Figure 8. a) Pyroelectric current **j** in sample ASN1 periodically heated with an IR laser as described in the Experimental section. Inset: showing the heating phase of the current decay which was used for fitting to the error function. The pyroelectric response is calculated from j_0. [22, 23]. b) Schematic of sample ASN1 as prepared for these measurements with a 2mm diameter , black paint-coated upper Ti electrode.

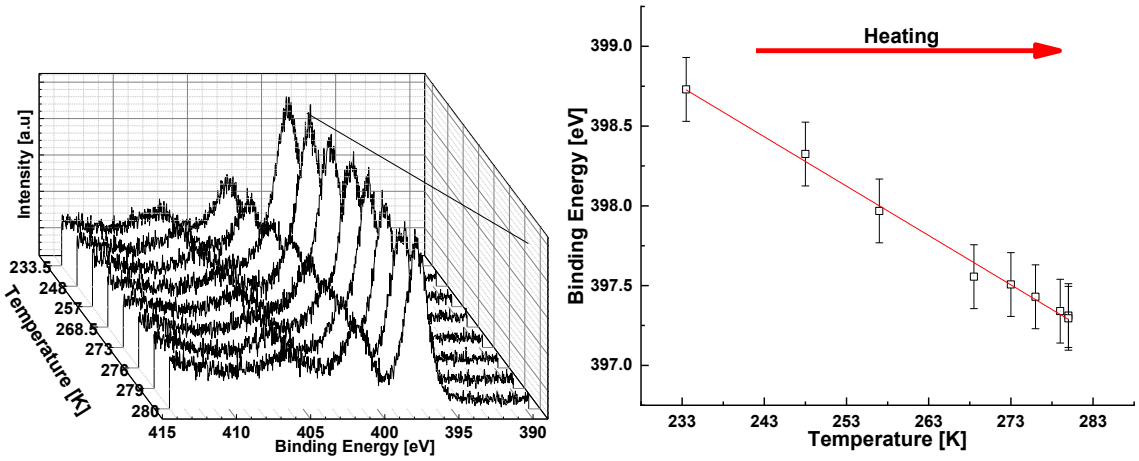

(a) *(b)*

Figure 9. a) XPS measurement of the N 1s spectrum under controlled temperature change (233-280K) of the ASN1 sample ; b) N 1s peak positions as a function of temperature during heating in ultra-high vacuum. The monotonic shift to lower binding energies upon heating indicates electron accumulation, which is consistent with Al-termination [24]. Error bars indicate experimental uncertainty.

3.4 Measurement of the piezoelectric coefficient

The current detected during the piezoelectric response measurements was very small (1-20nA), evidence that the cantilevers were not shorted. The mean converse transversal piezoelectric coefficient calculated from the cantilever deflection amplitude and averaged over three cantilevers cut from the same Si wafer, was $e_{31} = 1.58 \pm 0.14 C/m^2$. (Figure 10 and Supplementary, Section S6). This value is similar to those reported in the literature for films with the same Sc concentration (25mol% Sc) but < 1 µm thick [43]. Thus, with our preparation protocol, increase in thickness does not cause deterioration of the piezoelectric coefficient. Similarly, the dielectric permittivity of the AlScN films, as measured by impedance spectroscopy at 0.5Hz, 0.1Vac, is $\varepsilon_r = 12.5 \pm 1.0$ in agreement with refs. [43] , [44].

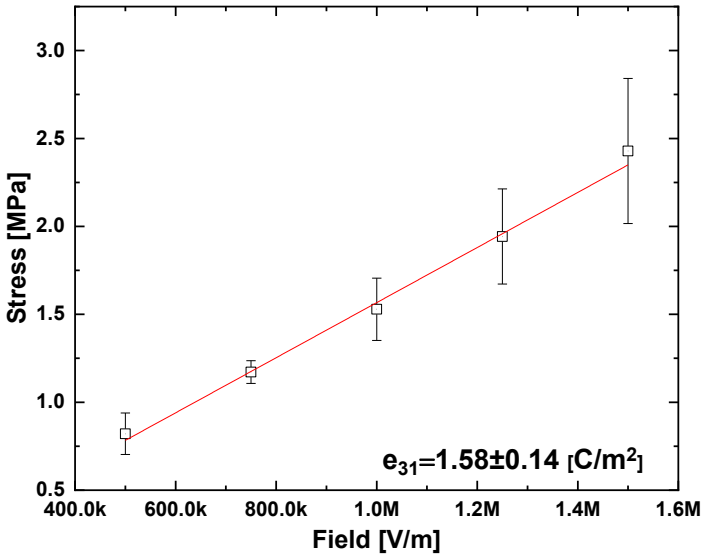

Figure 10. Dependence of quasi-static (0.1 Hz) stress *vs* electric field for ASN1 sample cantilevers fabricated from a single Si wafer and quantitated by cantilever (substrate) deflection in response to the electric field applied perpendicular to the plane of the cantilever, along with knowledge of thickness and mechanical properties of the wafer and film.

4. Summary

In summary, a protocol for successfully depositing stable, [*00l*] textured, 2-3μm thick films of $Al_{0.75}Sc_{0.25}N$, is described. The procedure exploits the formation of sputtered, ***α***-phase (hcp) Ti thin films with (00*l*)-texture. We present evidence that chemical reaction between (00*l*)-textured α-Ti and nitrogen plasma during reactive sputtering of (Al,Sc)N leads to the rapid formation of an intervening, very thin TiN seeding layer, presenting lattice mismatch of only 3.7% between the (111) planes of TiN and the (001) planes of the $Al_{0.75}Sc_{0.25}N$ film. This is up to three times smaller mismatch than that presented by inert metal seeding layers commonly used for film preparation. We suggest that it is this close lattice match that is an important determinant for the low values of deposition compressive stress, $\sigma_f <$ 100MPa , maintained in spite of the thickness of the (Al,Sc)N film. In contrast to earlier reports, the $Al_{0.75}Sc_{0.25}N$ films prepared in the current study are polar with [00**l**] orientation rather than [00$\bar{\mathbf{1}}$]: this is consistent with growth initiation on a nitrogen layer. Although 2-3 μm thick, these films display pyroelectric and piezoelectric coefficients similar to those reported for significantly thinner films (< 1 μm) [8, 39]. An important practical advantage of the proposed growth technique is its compatibility with a variety of substrates commonly used for actuators or MEMS, as demonstrated here for both Si wafers and D263 borosilicate glass. Additionally, thicker films can potentially achieve increased piezoelectric stress/strain by permitting application of higher voltage, but without increase in the magnitude of the electric field.

5.Patents

A patent application based on the data reported in this article has been submitted and approval is pending .

Supplementary Materials: The following supporting information can be downloaded at: www.mdpi.com/xxx/s1, Section S1: Epitaxial relationships between hcp *(00l)* oriented Ti; cubic (111) oriented TiN; and hcp *(00l)* oriented AlN.; Section S2: XRD profiles and pole figures of textured *(00l)* Ti and (111) TiN on Si.; Section S3: EDS elemental analysis of (Al,Sc)N film stoichiometry, sputtered from a single $Al_{0.75}Sc_{0.25}$ alloy target **;** Section S4**:** Temperature optimization for textured (Al,Sc)N deposition.; Section S5: Calculating the film pyroelectric coefficient α_f from error function fitting; Section 6: Transversal, converse piezoelectric coefficient e_{31} for AlScN thin films, evaluated for three rectangular cantilevers fabricated on the surface of the same Si wafer.

Author Contributions: A.C., S.K., I.L. and D.E. conceived and designed the experiment; A.C. prepared the samples and performed the experiments; H.C. performed the XPS measurements; S.R.C. performed the AFM measurements; A.C., Y.F. and A.K. performed the XRD measurements; A.C., and D.E. performed the pyroelectric measurements; A.C., I.K.A. and A.K. performed the SEM measurements; A.C. and S.K. performed piezoelectric measurements; D.E., A.C. and I.L. analyzed the data and prepared the original draft; A.I.F. and E.W. discussed, reviewed and edited the draft; All authors have read and agreed to the published version of the manuscript.

Funding: This work was supported by NATO Science for Peace award G5453, and, in part, by the BioWings project, which has received funding from the European Union Horizon 2020 under the Future and Emerging Technologies (FET) program with grant agreement No 801267. IL and AIF acknowledge the NSF-BSF program grant 2018717. AIF acknowledges support by U. S. National Science Foundation Grant number DMR-1911592.

Institutional Review Board Statement: Not applicable.

Informed Consent Statement: Not applicable**.**

Data Availability Statement: The data presented in this study are available on request from the corresponding author**.**

Acknowledgments: Not applicable.

Conflicts of Interest: The authors declare no conflict of interest.

References

1. Aigner, R.; Kaitila, J.; Ella, J.; Elbrecht, L.; Nessler, W.; Handtmann, M.; Herzog, T. R.; Marksteiner, S., Bulk-acoustic-wave filters: Performance optimization and volume manufacturing. *2003 Ieee Mtt-S International Microwave Symposium Digest, Vols 1-3* **2003**, 2001-2004.
2. Elfrink, R.; Kamel, T. M.; Goedbloed, M.; Matova, S.; Hohlfeld, D.; van Andel, Y.; van Schaijk, R., Vibration energy harvesting with aluminum nitride-based piezoelectric devices. *Journal of Micromechanics and Microengineering* **2009,** 19, (9), 094005.
3. Sandu, C. S.; Parsapour, F.; Mertin, S.; Pashchenko, V.; Matloub, R.; LaGrange, T.; Heinz, B.; Muralt, P., Abnormal Grain Growth in AlScN Thin Films Induced by Complexion Formation at Crystallite Interfaces. *Physica Status Solidi a-Applications and Materials Science* **2019,** 216, (2), 1800569.
4. Akiyama, M.; Kano, K.; Teshigahara, A., Influence of growth temperature and scandium concentration on piezoelectric response of scandium aluminum nitride alloy thin films. *Applied Physics Letters* **2009,** 95, (16), 162107.
5. Schuster, J. C.; Bauer, J., The Ternary-Systems Sc-Al-N and Y-Al-N. *Journal of the Less-Common Metals* **1985,** 109, (2), 345-350.
6. Akiyama, M.; Nagao, K.; Ueno, N.; Tateyama, H.; Yamada, T., Influence of metal electrodes on crystal orientation of aluminum nitride thin films. *Vacuum* **2004,** 74, (3-4), 699-703.
7. Iriarte, G. F.; Bjurstrom, J.; Westlinder, J.; Engelmark, F.; Katardjiev, I. V., Synthesis of c-axis-oriented AlN thin films on high-conducting layers: Al, Mo, Ti, TiN, and Ni. *Ieee Transactions on Ultrasonics Ferroelectrics and Frequency Control* **2005,** 52, (7), 1170-1174.
8. Mertin, S.; Heinz, B.; Rattunde, O.; Christmann, G.; Dubois, M. A.; Nicolay, S.; Muralt, P., Piezoelectric and structural properties of c-axis textured aluminium scandium nitride thin films up to high scandium content. *Surface & Coatings Technology* **2018,** 343, 2-6.
9. Artieda, A.; Barbieri, M.; Sandu, C. S.; Muralt, P., Effect of substrate roughness on c-oriented AlN thin films. *Journal of Applied Physics* **2009,** 105, (2), 024504.

10. Moram, M. A.; Zhang, S., ScGaN and ScAlN: emerging nitride materials. *Journal of Materials Chemistry A* **2014,** 2, (17), 6042-6050.
11. Esteves, G.; Berg, M.; Wrasman, K. D.; Henry, M. D.; Griffin, B. A.; Douglas, E. A., CMOS compatible metal stacks for suppression of secondary grains in Sc0.125Al0.875N. *Journal of Vacuum Science & Technology A* **2019,** 37, (2), 021511.
12. Bogner, A.; Timme, H. J.; Bauder, R.; Mutzbauer, A.; Pichler, D.; Krenzer, M.; Reccius, C.; Weigel, R.; Hagelauer, A., Impact Of High Sc Content On Crystal Morphology And RF Performance Of Sputtered Al1-xScxN SMR BAW. *2019 Ieee International Ultrasonics Symposium (Ius)* **2019**, 706-709.
13. Shao, S.; Luo, Z. F.; Wu, T., High Figure-of-Merit Lamb Wave Resonators Based on Al0.7Sc0.3N Thin Film. *Ieee Electron Device Letters* **2021,** 42, (9), 1378-1381.
14. Shao, S.; Luo, Z. F.; Lu, Y.; Mazzalai, A.; Tosi, C.; Wu, T., High Quality Co-Sputtering AlScN Thin Films for Piezoelectric Lamb-Wave Resonators. *Journal of Microelectromechanical Systems* **2022,** 31, (3), 328-337.
15. Beaucejour, R.; Roebisch, V.; Kochhar, A.; Moe, C. G.; Hodge, M. D.; Olsson, R. H., Controlling Residual Stress and Suppression of Anomalous Grains in Aluminum Scandium Nitride Films Grown Directly on Silicon. *Journal of Microelectromechanical Systems* **2022**.
16. Rassay, S.; Hakim, F.; Li, C.; Forgey, C.; Choudhary, N.; Tabrizian, R., A Segmented-Target Sputtering Process for Growth of Sub-50 nm Ferroelectric Scandium-Aluminum-Nitride Films with Composition and Stress Tuning. *Physica Status Solidi-Rapid Research Letters* **2021,** 15, (5), 2100087.
17. Chen, A. Y.; Bu, Y.; Tang, Y. T.; Wang, Y.; Liu, F.; Xie, X. F.; Gu, J. F., Deposition-rate dependence of orientation growth and crystallization of Ti thin films prepared by magnetron sputtering. *Thin Solid Films* **2015,** 574, 71-77.
18. Chawla, V.; Jayaganthan, R.; Chawla, A. K.; Chandra, R., Microstructural characterizations of magnetron sputtered Ti films on glass substrate. *Journal of Materials Processing Technology* **2009,** 209, (7), 3444-3451.
19. Chun, J. S.; Petrov, I.; Greene, J. E., Dense fully 111-textured TiN diffusion barriers: Enhanced lifetime through microstructure control during layer growth. *Journal of Applied Physics* **1999,** 86, (7), 3633-3641.
20. Korobko, R.; Patlolla, A.; Kossoy, A.; Wachtel, E.; Tuller, H. L.; Frenkel, A. I.; Lubomirsky, I., Giant Electrostriction in Gd-Doped Ceria. *Advanced Materials* **2012,** 24, (43), 5857-5861.
21. Lubomirsky, I.; Stafsudd, O., Invited Review Article: Practical guide for pyroelectric measurements. *Review of Scientific Instruments* **2012,** 83, (5), 121101.
22. Ehre, D.; Mirzadeh, E.; Stafsudd, O.; Lubomirsky, I., Pyroelectric Measurement of Surface Layer: The Case of Thin Film on Dielectric Substrate. *Ferroelectrics* **2014,** 472, (1), 41-49.
23. Ehre, D.; Lyahovitskaya, V.; Tagantsev, A.; Lubomirsky, I., Amorphous piezo- and pyroelectric phases of BaZrO3 and SrTiO3. *Advanced Materials* **2007,** 19, (11), 1515-1516.
24. Ehre, D.; Cohen, H., Contact-free pyroelectric measurements using x-ray photoelectron spectroscopy. *Applied Physics Letters* **2013,** 103, (5), 052901.
25. Whatmore, R. W., Pyroelectric Devices and Materials. *Reports on Progress in Physics* **1986,** 49, (12), 1335-1386.
26. Damjanovic, D., Ferroelectric, dielectric and piezoelectric properties of ferroelectric thin films and ceramics. *Reports on Progress in Physics* **1998,** 61, (9), 1267-1324.
27. Milosev, I.; Strehblow, H. H.; Navinsek, B.; Metikoshukovic, M., Electrochemical and Thermal-Oxidation of Tin Coatings Studied by Xps. *Surface and Interface Analysis* **1995,** 23, (7-8), 529-539.
28. Chan, M. H.; Lu, F. H., X-ray photoelectron spectroscopy analyses of titanium oxynitride films prepared by magnetron sputtering using air/Ar mixtures. *Thin Solid Films* **2009,** 517, (17), 5006-5009.
29. Jaeger, D.; Patscheider, J., A complete and self-consistent evaluation of XPS Spectra of TiN. *Journal of Electron Spectroscopy and Related Phenomena* **2012,** 185, (11), 523-534.
30. Khandaker, M.; Riahinezhad, S.; Li, Y. L.; Vaughan, M. B.; Sultana, F.; Morris, T. L.; Phinney, L.; Hossain, K., Plasma nitriding of titanium alloy: Effect of roughness, hardness, biocompatibility, and bonding with bone cement. *Bio-Medical Materials and Engineering* **2016,** 27, (5), 461-474.
31. Kusmanov, S. A.; Smirnov, A. A.; Silkin, S. A.; Parfenyuk, V. I.; Belkin, P. N., Plasma electrolytic nitriding of alpha- and beta-titanium alloy in ammonia-based electrolyte. *Surface & Coatings Technology* **2016,** 307, 1291-1296.
32. Schulz, H.; Thiemann, K., Crystal structure refinement of AlN and GaN. *Solid State Communications* **1977,** 23, (11), 815-819.
33. Brozek, V.; Hajek, B.; Duvigneaud, P.-H., Dilatation thermique des produits d'oxydation du scandium. *Journal of The Less-Common Metals* **1973,** 33, (3), 385-386.
34. Mishin, S.; Gutkin, M.; Bizyukov, A.; Sleptsov, V., Method of Controlling Coupling Coefficient of Aluminum Scandium Nitride Deposition in High Volume Production. *2013 Joint European Frequency and Time Forum & International Frequency Control Symposium (Eftf/Ifc)* **2013**, 126.
35. Wang, D. X.; Zheng, J.; Tang, Z. C.; D'Agati, M.; Gharavi, P. S. M.; Liu, X. W.; Jariwala, D.; Stach, E. A.; Olsson, R. H.; Roebisch, V.; Kratzer, M.; Heinz, B.; Han, M. G.; Kisslinger, K., Ferroelectric C-Axis Textured Aluminum Scandium Nitride Thin Films of 100 nm Thickness. *2020 Joint Conference of the Ieee International Frequency Control Symposium and International Symposium on Applications of Ferroelectrics (Ifcs-Isaf)* **2020**, 1-4.

36. Park, M.; Hao, Z. J.; Dargis, R.; Clark, A.; Ansari, A., Epitaxial Aluminum Scandium Nitride Super High Frequency Acoustic Resonators. *Journal of Microelectromechanical Systems* **2020,** 29, (4), 490-498.
37. Ehre, D.; Cohen, H.; Lyahovitskaya, V.; Lubomirsky, I., X-ray photoelectron spectroscopy of amorphous and quasiamorphous phases of BaTiO(3) and SrTiO(3). *Physical Review B* **2008,** 77, (18), 184106.
38. Meirzadeh, E.; Christensen, D. V.; Makagon, E.; Cohen, H.; Rosenhek-Goldian, I.; Morales, E. H.; Bhowmik, A.; Lastra, J. M. G.; Rappe, A. M.; Ehre, D.; Lahav, M.; Pryds, N.; Lubomirsky, I., Surface Pyroelectricity in Cubic SrTiO3. *Advanced Materials* **2019,** 31, (44), 1904733.
39. Kurz, N.; Lu, Y.; Kirste, L.; Reusch, M.; Zukauskaite, A.; Lebedev, V.; Ambacher, O., Temperature Dependence of the Pyroelectric Coefficient of AlScN Thin Films. *Physica Status Solidi a-Applications and Materials Science* **2018,** 215, (13), 1700831.
40. Gaur, S. P.; Rangra, K.; Kumar, D., MEMS AlN pyroelectric infrared sensor with medium to long wave IR absorber. *Sensors and Actuators a-Physical* **2019,** 300, 111660.
41. Bette, S.; Fichtner, S.; Broker, S.; Nielen, L.; Schmitz-Kempen, T.; Wagner, B.; Van Buggenhout, C.; Tiedke, S.; Tappertzhofen, S., Infrared-laser based characterization of the pyroelectricity in AlScN thin-films. *Thin Solid Films* **2019,** 692, 137623.
42. Tappertzhofen, S.; Bette, S.; Sievers, F.; Fichtner, S.; Broker, S.; Schmitz-Kempen, T., Sub-micrometer pyroelectric tomography of AlScN films. *Applied Physics Letters* **2021,** 118, (24), 242901.
43. Akiyama, M.; Umeda, K.; Honda, A.; Nagase, T., Influence of scandium concentration on power generation figure of merit of scandium aluminum nitride thin films. *Applied Physics Letters* **2013,** 102, (2), 021915.
44. Fichtner, S.; Reimer, T.; Chemnitz, S.; Lofink, F.; Wagner, B., Stress controlled pulsed direct current co-sputtered Al1-xScxN as piezoelectric phase for micromechanical sensor applications. *Apl Materials* **2015,** 3, (11), 116102.